RESEARCH ARTICLE

Impregnation of biochar with montmorillonite and its activation for the removal of azithromycin from aqueous media

Muhammad Arif[1,2] · Guijian Liu[1,3] · Muhammad Zia ur Rehman[4] · Md Manik Mian[1] · Aniqa Ashraf[1] · Balal Yousaf[1] · Muhammad Saqib Rashid[1] · Rafay Ahmed[1] · Muhammad Imran[5] · Mehr Ahmed Mujtaba Munir[6]

Abstract

An inexpensive and environmentally friendly composite synthesized from rice husk, impregnated with montmorillonite and activated by carbon dioxide, was investigated for the removal of azithromycin from an aqueous solution. Various techniques were used to characterize adsorbents in detail. The sorption process was primarily regulated by the solution pH, pollutant concentration, contact duration, adsorbent dose, and solution temperature. The equilibrium data were best analyzed using the nonlinear Langmuir and Sips ($R^2 > 0.97$) isotherms, which revealed that adsorption occurs in a homogenous manner. The adsorption capacity of pristine biochar and carbon dioxide activated biochar-montmorillonite composite was 33.4 mg g^{-1} and 44.73 mg g^{-1}, respectively. Kinetic studies identified that the experimental data obeyed the pseudo-second-order and Elovich models ($R^2 > 0.98$) indicating the chemisorption nature of adsorbents. The thermodynamic parameters determined the endothermic and spontaneous nature of the reaction. The ion exchange, π-π electron-donor–acceptor (EDA) interactions, hydrogen-bonding, and electrostatic interactions were the plausible mechanisms responsible for the adsorption process. This study revealed that a carbon dioxide activated biochar-montmorillonite composite may be used as an effective, sustainable, and economical adsorbent for the removal of azithromycin from polluted water.

Responsible Editor: Tito Roberto Cadaval Jr

✉ Guijian Liu
  lgj@ustc.edu.cn

1 CAS Key Laboratory of Crust-Mantle Materials and Environment, School of Earth and Space Sciences, University of Science and Technology of China, Hefei, Anhui 230026, People's Republic of China

2 Department of Soil and Environmental Sciences, MNS University of Agriculture, Multan 60000, Pakistan

3 State Key Laboratory of Loess and Quaternary Geology, Institute of Earth Environment, The Chinese Academy of Sciences, Xi'an 710075, Shaanxi, China

4 Institute of Soil and Environmental Sciences, University of Agriculture, Faisalabad 38040, Pakistan

5 Nuclear Institute for Agriculture and Biology (NIAB), Jhang Road, Faisalabad 38000, Pakistan

6 Ministry of Education (MOE) Key Laboratory of Environmental Remediation and Ecosystem Health, College of Environmental and Resources Science, Institute of Crop Science and Zhejiang Key Laboratory of Crop Germplasm, Zhejiang University, Zhejiang University, Hangzhou 310058, China

Abbreviations

AZT	Azithromycin
COVID-19	Coronavirus disease 2019
BC	Biochar
CO_2	Carbon dioxide
ABC	CO_2 activated biochar
MBC	Montmorillonite biochar composite
AMBC	CO_2 activated montmorillonite biochar composite
MMT	Montmorillonite
HCl	Hydrochloric acid
NaOH	Sodium hydroxide
AR	Analytical reagent grade
DI	Deionized water
mL	Milli liter
min.	Minute
sec	Second
XPS	X-ray photoelectron spectroscopy
XRD	X-ray diffraction
SEM	Scanning electron microscope
EDS	Energy dispersive X-ray spectrometry
TGA	Thermogravimetric analysis

DTGA	Derived Thermogravimetric Analysis
BET	Brunauer-Emmett-Teller
EPR	Electron paramagnetic resonance
FTIR	Fourier transform infrared spectroscopy
PD	Pore diameter
TPV	Total pore volume
SSA	Specific surface area
PFO	Pseudo-first-order
PSO	Pseudo-second-order
DMPO	5,5-Dimethyl-1-pyrroline N-oxide
TBA	Tert-butylalcohol

Introduction

Antibiotics account for 15% of all the pharmaceutical compounds produced throughout the world (Talaiekhozani et al. 2020). They can be divided into different groups such as sulfonamides, quinolones, β-lactams, tetracyclines, aminoglycosides, and macrolides based on their chemical structure and mechanism (Davoodi et al. 2019). Only a small portion of the administered antibiotics is absorbed by the body, while a substantial fraction is released unchanged through urine and feces into the environment. This can affect the population of microorganisms in the environment, contributing to the emergence of resistant strains. Furthermore, they pose potentially toxic risks to aquatic organisms and may be absorbed eventually by humans through the food chain and drinking water (Ashraf et al. 2022; Yi et al. 2016).

Among different types of antibiotics, azithromycin (AZT) is a second-generation novel macrolide antibiotic (Saadi et al. 2020), has a broad spectrum (Li et al. 2021) and superior acid stability. It is a semisynthetic derivative of erythromycin (Chang et al. 2015) that was produced to overcome erythromycin shortcomings (Davoodi et al. 2019). The AZT not only acts as an active agent in curing diseases caused by a variety of Gram-positive and Gram-negative bacteria but it can also be used effectively against atypical pathogens (Xiang et al. 2020), which has pushed for its usage in the prevention of a variety of respiratory as well as reproductive health diseases (Cano et al. 2020). Although AZT is an antibiotic but it is one of the most successful and widely prescribed medicines for coronavirus disease 2019 (COVID-19) therapy. One hospital in Brazil reported a 2500% rise in the rate of AZT use in the emergency department during COVID-19, while another hospital in Brazil reported a 2000% increase in the rate of AZT consumption in the clinical ward during COVID-19 (Silva et al. 2021). It is difficult to know how much AZT was prescribed during COVID-19 in the United States (US), however the use of AZT was so high that there was a shortage. The United States Environmental Protection Agency recognized the AZT as a contaminant of emerging concern (Vermillion Maier and Tjeerdema

2018) because its presence might cause severe threats to flora and fauna, including humans (Archer et al. 2017). It has been included in the European Union Watch List of potentially hazardous compounds for the aquatic environment (Senta et al. 2019).

Owing to limited absorption and negligible metabolic rate, 70% of AZT is excreted from the body predominantly unchanged (Davoodi et al. 2019). As a result, AZT may eventually be found in wastewater and water resources (Alves et al. 2018; Hanamoto and Ogawa 2019). The introduction of AZT into natural water sources has the potential to alter the native microbial populations and promote the selection of resistant bacterial strains, which can then trigger diseases that are resistant to traditional antibiotics, leading to the antibiotic-resistant epidemic (Cano et al. 2020). The accumulation of AZT in the aquatic system due to its persistent nature and structural stability for a more extended period poses severe threats to human health and the environment (Sobhan Ardakani et al. 2020). Hence, the removal of AZT from water and wastewater is of great significance.

Up to now, several methods have been tested by researchers to eliminate AZT from contaminated water, including adsorption (Ma et al. 2021), membrane separation (Avella et al. 2010), chemical oxidation (Li et al. 2019), photocatalytic degradation (Ashraf et al. 2021), and biological means to treat AZT (Alvarino et al. 2017; Yang et al. 2017). However, adsorption acquires particular importance since it is considered the most promising technology because of its high efficiency, low cost (Sophia and Lima 2018), convenience, simple design, and because it does not add unwelcome byproducts to the system (Andrade et al. 2018; Arif et al. 2021). Although, a variety of adsorbents have been extensively employed, including activated carbon (Gupta and Garg 2019), graphene, resins, carbon nanotubes, fly ash (Zhang et al. 2011), soil (Carrasquillo et al. 2008) and mineral oxides (Yin et al. 2018) to remove AZT from wastewater, their application has been limited due to cost-effectiveness and adsorption performance (Huang et al. 2020). Hence, when selecting a new adsorbent, it must be considered that the selected adsorbent should have a high surface area, be eco-friendly, have a well-developed porous structure, have modified surface functional groups, be readily available, and be inexpensive.

Biochar (BC), a carbonaceous material produced from biomass in an oxygen limited environment, has recently gained momentum over activated carbon and is being investigated as an alternative adsorbent for remediation of AZT. Even though BC is less expensive than activated carbon, the ionic size of AZT does not fit into the pore size of BC and the ionic nature of antibiotics causes electrostatic repulsion. These properties limit the adsorption capacity (Ashiq et al. 2019a; Peng et al. 2016).

The activation of BC with carbon dioxide (CO_2) has been proposed to boost its surface characteristics, including porosity and surface area, therefore making it a very efficient adsorbent for the removal of different pollutants (Kołtowski et al. 2017; Sun et al. 2020). Likewise, coating clay minerals onto BC to create BC-clay mineral composites has received attention to change the surface characteristics of BC and absorb various pollutants (Yao et al. 2014).

The clay minerals have been extensively studied for sorptive removal of antibiotics due to their high cation exchange capacity, layered structure, large surface area, and chemical/mechanical stability (Viglašová et al. 2018). Montmorillonite (MMT) has received a lot of interest among the clay minerals because of its abundance, low cost, and promising features including high porosity, mechanical strength, and cation exchange capacity (Zango et al. 2022). The MMT is a 2:1 aluminosilicate clay mineral in which cations in the interlayer gaps are replaced by positively charged contaminants through a cation exchange process. MMT also has a high swelling capacity. These characteristics make it an excellent choice for wastewater cleanup applications (Zango et al. 2022). It has a higher ion exchange capacity (60–170 meq/100 g) than other related clay minerals. Moreover, MMT itself contains metal atoms of aluminum, magnesium, and these exogenous metal atoms may be embedded therein to react with BC, enhancing the performance of the MMT-BC composite (MBC) (Song et al. 2020).

Hence, the modification of rice husk-BC with MMT was considered to be a good option for the adsorption of AZT. Further, it was also observed in some studies that clay minerals had reduced the surface area of BC by obstructing the surface pores (Rawal et al. 2016). So, keeping in mind the above limitation, activation of the BC-clay mineral composite was done using CO_2 to enhance its porosity for improved adsorption. This study evaluated the AZT removal from contaminated water using CO_2 activated BC-MMT composite (AMBC), which has not been considered before to the best of our knowledge. The characterization of adsorbents and plausible mechanisms for AZT adsorption were studied.

Materials and methods

Materials and chemicals

The AZT was purchased from Shanghai Aladdin Biochemical Technology. The rice husk (RH) used in this study was obtained from a farm near Hefei, China. Southern Clay Products Inc supplied the MMT. Alfa Aesar (China) Chemicals Co. Ltd provided methanol (CH_4O), hydrochloric acid (HCl) and sodium hydroxide (NaOH). All the experimental solutions were prepared using analytical reagent grade (AR) chemicals without further purification and ultrapure deionized water (Milli-Q/18.2 MΩ cm).

Synthesis and modification of BC, ABC, MBC and AMBC

After washing the rice husk biomass, it was air-dried, ground, transferred into a crucible and placed into a tube furnace at a pyrolysis temperature of 500 °C with a heating rate of 10 °C min^{-1} using N_2 as inert gas for 60 min retention time. The N_2 gas was replaced with CO_2 (800 ml min^{-1}) to activate the BC with CO_2 to enhance its surface properties after the desired temperature was achieved. The CO_2 gas was then switched back to N_2 after 60 min of retention time to allow the system to cool.

For the preparation of ABC, 50 g of MMT powder was mixed with 2 L of water and sonicated for 30 min by using ultrasonicator (Rocker-Soner 220). This resulted in a homogeneous mixture, which was then placed on a mechanical shaker for 4 h. Then, 150 g of prepared rice husk BC at 500 °C was mixed and shaken for further 4 h. The BC-MMT slurry was then filtered using 0.45-μm syringe filter after centrifugation and kept in an oven at 80 °C overnight. Furthermore, the composite was sieved through a 100 mm mesh before the experiment. This prepared MBC was kept in a tube furnace in the presence of N_2 at 500 °C and after attaining the desired temperature, N_2 was switched to CO_2 (1000 mL min^{-1}) gas for activation of the MBC for a 60 min retention time. The CO_2 was converted back to N_2 when the retention time was completed, and the system was cooled. The characterization detail of the adsorbents is given in section 1 of the supplementary material.

Batch experiment

All the prepared adsorbent materials were tested to investigate the removal of AZT from contaminated water. The adsorbent dose of 1 g L^{-1} against a 25 mg L^{-1} solution concentration of AZT at neutral pH in a typical batch test. The flasks containing these solutions were placed on the mechanical shaker with a shaking speed of 150 rpm at room temperature (22 ± 0.5 °C) and adsorption equilibrium was reached after 6 h. After achieving equilibrium, the supernatant was filtered through a 0.22 μm syringe filter and subjected to a UV–vis spectrophotometer for AZT at a wavelength of 452 nm, as established in the previous work (Ashour and Bayram 2012). We investigated the influence of pH on AZT adsorption by varying pH, which varied from 3.0 to 11.0 while the other parameters remained constant. The suspensions were taken at various contact times including 5, 15, 30, 60, 120, 240, 360, 480, 600, and 720 min for kinetic studies. Following each run, the AZT concentration

was determined as mentioned before. The adsorption experiments were carried out and the AZT concentration used for adsorption models was in the range of 10–400 mg L^{-1} maintaining neutral pH for 360 min while keeping all other parameters constant.

Adsorption analyses

The non-linear forms of adsorption isotherms and kinetics were used. For kinetic studies, non-linear kinetic models such as pseudo-first-order (PFO), pseudo-second-order (PSO), and Elovich model were used. The kinetic parameters and error analysis were estimated using nonlinear regression and the SigmaPlot 11 software. The nonlinear PFO equation is given below (Eq. 1) (Ouasfi et al. 2019).

$$q_t = q_e(1 - e^{-k_1 t}) \tag{1}$$

where q_t is the adsorption capacity (mg g^{-1}) at time t, q_e is the adsorption capacity (mg g^{-1}) at equilibrium and the rate constant is k_1 (min^{-1}).

The nonlinear PSO equation is given below (Eq. 2) (Ashiq et al. 2019b; Wu et al. 2014).

$$q_t = \frac{q_e t}{\left(1/k_2 q_e\right) + t} \tag{2}$$

whereas, k_2 (kg g^{-1} min^{-1}) is the rate constant of the PSO equation.

The non-linear Elovich equation is the below equation (Eq. 3) (Wu et al. 2009, 2014).

$$q_t = \left(\frac{1}{v}\right)\ln(uv) + \left(\frac{1}{v}\right)lnt \tag{3}$$

where, u and v are constants throughout the experiment, and u is taken to represent the initial rate (kg g^{-1} min^{-1}), while v is desorption constant (g mg^{-1}) and it can be determined according to measurement.

The Langmuir, Freundlich, Sips, and Redlich-Peterson isotherm models were used to know the adsorption of AZT by different adsorbents. The Langmuir equation has the following nonlinear form (Langmuir 1916; Huang et al. 2020)

$$q_e = \frac{K_L q_{m,L} C_e}{1 + K_L C_e} \tag{4}$$

where, q_e describes the adsorption capacity of AZT at equilibrium (mg g^{-1}); K_L (m^3 g^{-1}) is constant; $q_{m,L}$ is the maximum adsorption capacity (mg g^{-1}); C_e is the equilibrium concentration of AZT (mg L^{-1});

Freundlich equation has a nonlinear version that may be expressed as (Dehghan et al. 2019):

$$q_e = K_F C_e^{1/n_F} \tag{5}$$

q_e is the equilibrium adsorption capacity (mg g^{-1}), 1/n and K_F are Freundlich empirical constants, C_e expresses the equilibrium concentration (mg L^{-1}). Freundlich constant has no unit. They are achieved while plotting adsorption data.

The equation of Sips adsorption isotherm model can be written as (Wu et al. 2014)

$$q_e = \frac{q_{m,S}(K_S C_e)^{1/n_S}}{1 + (K_S C_e)^{1/n_S}} \tag{6}$$

$q_{m,s}$ is the adsorption capacity (g kg^{-1}) derived from Sips equation, K_s is Sips isotherm model constant (m^3 g^{-1})$^{1/n}$s, and $1/n_S$ is Sips isotherm model exponent.

Results and discussions

Characterization

The SEM images of the synthesized materials are shown in Fig. 1. The surface morphology of BC and ABC is smooth compared to MBC and AMBC. This clearly showed that the MMT particles attached to the BC surface provided more surface areas and a rougher appearance for the adsorption of AZT. Pores can be observed in all the materials, which facilitate the removal of AZT via enhanced surface adsorption through pore-filling mechanisms. However, coating with MMT could cause clogging of pores that might lead to decreased removal of AZT. This can be increased through the activation of CO$_2$, as can be seen in AMBC. These results are consistent with the previous study (Yao et al. 2014). The BC derived from rice husk is rich in Si and N and preserve these elements within their structures (Feng et al. 2021; Hossain et al. 2020; Vikrant et al. 2022). The surface coverage of these BCs with MMT was further confirmed to visualize the elemental distribution on the surfaces of the analyzed materials with Energy Dispersive X-ray Spectrometry (EDS) analysis, as shown in Fig. S2. Following our assumptions, the EDS spectrum and SEM analysis revealed that the elements C, O, Si, and Al were dispersed throughout all of the studied materials, with the highest peaks corresponding to Al and Si, which is characteristic of MMT.

The elemental composition presented in Table 1 showed that C content was much lower in MBC and AMBC as compared to BC, though it was slightly higher in ABC.

The reason for overall reduced C level in the composite was the addition of MMT. As MMT do not contain carbon the overall C content of the composite therefore remained unchanged. Similarly, H and O contents were decreased in composite materials, including MBC and AMBC, whereas there was a slight increase in ABC. The N content was

Fig. 1 The SEM images (magnification 500X) of BC (**A**), ABC (**B**), MBC (**C**), and AMBC (**D**) prepared at pyrolysis temperature of 500 °C
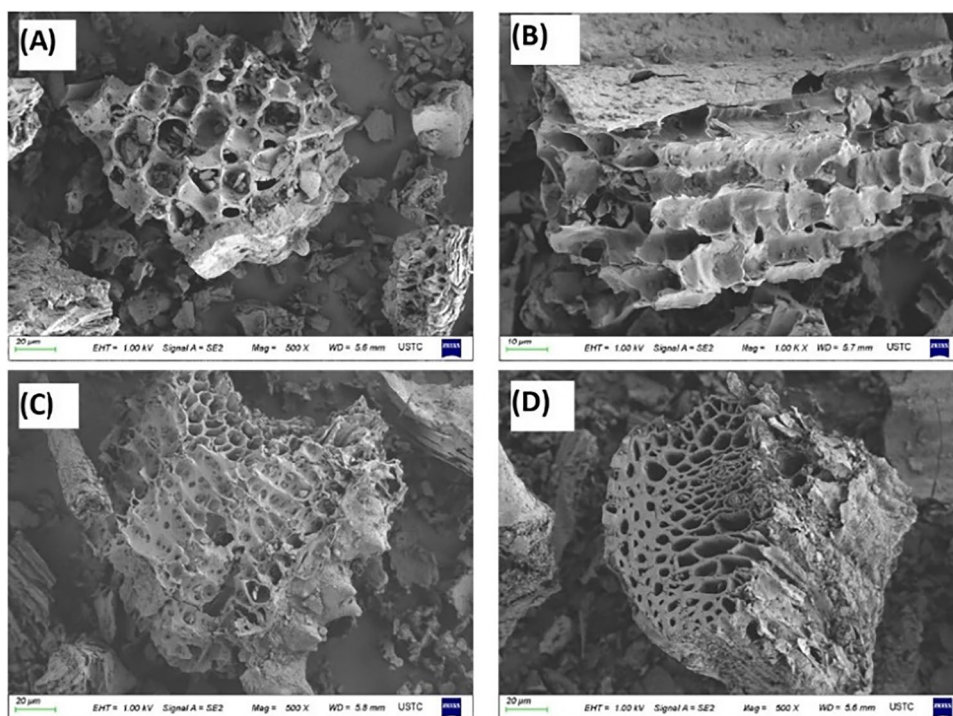

Table 1 Elemental composition, SSA_{BET}, TPV, and APW of MMT, BC, ABC, MBC, and AMBC synthesized at pyrolysis temperature of 500 °C

| Adsorbent	Elemental analysis				BET analysis		
	N (%)	C (%)	H (%)	O (%)	SSA_{BET} (m^2g^{-1})	TPV (cm^3g^{-1})	APW (Å)
MMT	0.00	0.00	1.60	11.29	15.37	0.06	143.14
BC	0.39	52.16	2.94	13.53	74.62	0.03	18.20
ABC	0.34	53.09	3.00	13.82	95.33	0.06	23.77
MBC	0.30	38.65	2.44	11.33	99.14	0.05	20.72
AMBC	0.36	38.67	2.45	11.90	127.16	0.01	23.08

comparatively higher in raw BC than in other adsorbents. Similarly, clay-mineral had a much higher average pore width (APW) (143.14 Å) than the other adsorbents, followed by AMBC (23.77 Å), ABC (23.08 Å), MBC (20.72 Å) and BC (18.20 Å). The range of BC yield from RH biomass was observed between 35–51% and there was an increasing trend with clay-mineral modification. However, a little decrease in yield was noted with CO_2 activation.

The SSA_{BET} and porosity analysis are summarized in Table 1. The high SSA_{BET} was found in the AMBC (127 m^2g^{-1}) followed by MBC (99 m^2g^{-1}), ABC (95 m^2g^{-1}), and BC (74 m^2g^{-1}), respectively. The SSA_{BET} of BC was shown to be higher after impregnation of MMT and CO_2 activation. The average pore width of the pure MMT was smaller as compared with all other carbonaceous materials and their composites (Yang et al. 2020). The N_2 adsorption/desorption curves in Fig. 2A shows that pristine BC adsorbed a low quantity of N_2 (17.37 cm^3g^{-1}) compared to its modified composites. The AMBC exhibited highest N_2 adsorption (71.58 cm^3g^{-1}), as compared to MBC-350 (45.00 cm^3g^{-1})

and ABC-350 (25.86 cm^3g^{-1}). According to International Union for Pure and Applied Chemistry classification, the as-synthesized materials display type II adsorption isotherm and H4-type hysteresis loop (Beltrame et al. 2018). Inconspicuous type II adsorption isotherms and H3-type hysteresis were observed in the MMT (Yang et al. 2020), confirming its macroporous or non-porous nature.

The Thermogravimetric Analysis (TGA) and Derived Thermogravimetric Analysis (DTGA) analyses are presented in Fig. 2B were conducted at a temperature range of 30 °C to 1000 °C in an N_2 atmosphere. The stability of MMT was highlighted, as its weight loss was less than 1% when heated below 100 °C. However, a rapid weight decline was observed from 349 °C to 600 °C, which might be due to the elimination of water by dehydration of exchangeable cations and tending to be stable after 806 °C. The loss in weight at a temperature higher than 600 °C could be attributed to the dehydroxylation of MMT (Zhou et al. 2012). The initial weight loss in the as-synthesized materials was almost 2–3% in the temperature range of 30–115 °C due

Fig. 2 N$_2$ adsorption-desorption curves (**A**), TGA/DTGA curves (**B**) and Raman analysis (**C**) of various adsorbents
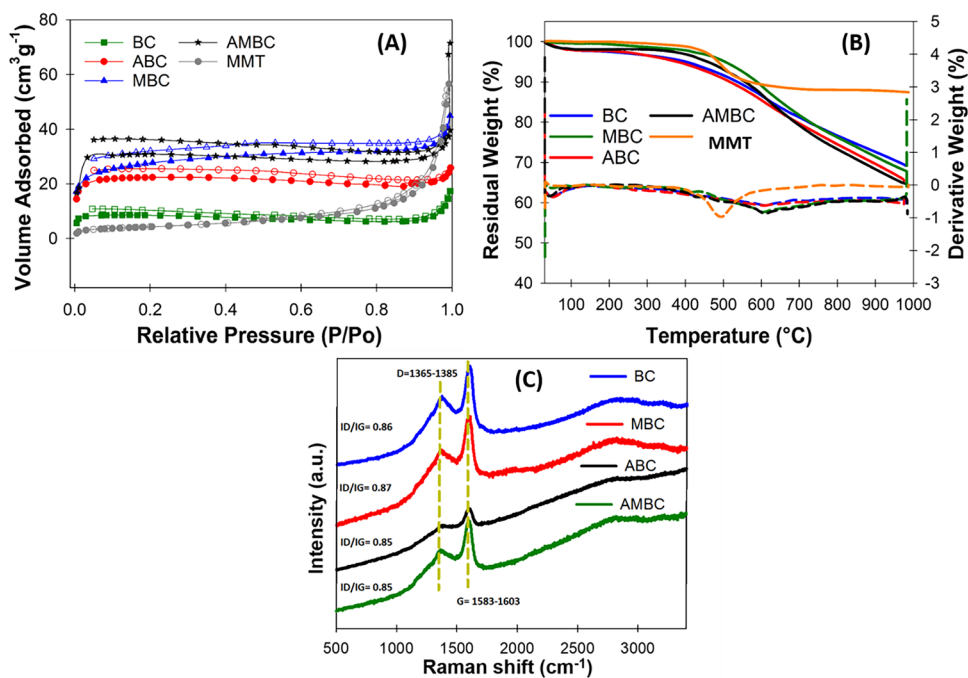

to evaporation of absorbed moisture. The second weight loss occurred because organic compounds like lignin, cellulose, and hemicellulose were broken down by the elevated temperature, which caused them to lose weight. The MBC showed enhanced stability, while it was slightly decreased in the AMBC (Amen et al. 2020; Lee et al. 2019). The DTGA curves for all adsorbents with dotted lines are illustrated in Fig. 2B, highlighting the weak peaks at 600 °C (Zhang et al. 2020).

The degree of graphitization and structural defects determined (Yang et al. 2020), using Raman spectroscopy are given in Fig. 2C. Two peaks at 1365–1385 cm^{-1} and 1583–1603 cm^{-1} were attributed to the D-band (which corresponds to a disordered carbon structure) and the G band (which corresponds to a sp2-hybridized graphitic carbon structure), (Zhang et al. 2018). Values of the *ID/IG* for BC, ABC, MBC, and AMBC, were 0.86, 0.85, 0.87, and 0.85, respectively. The Raman findings showed that pristine BC was mostly amorphous carbon with few defects. However, the modification of BC had no significant effect on the structure. The powdered X-ray Powder Diffraction (XRD) patterns of all the adsorbents (with and without AZT treatment) in the 2θ range of 10 to 80° are presented in Fig. 3. The modified BC demonstrated MMT deposition, indicating that it was loaded successfully. The d-values and reflection angles were slightly changed in the modified adsorbents. This change was ascribed to surface adsorbed water, leading to shrinkage of MMT and influencing its internal structure during pyrolysis treatment. The d-value of different adsorbents was shown to increase after the adsorption of AZT.

Fig. 3 XRD analysis of different adsorbents before (**A**) and after (**B**) AZT adsorption
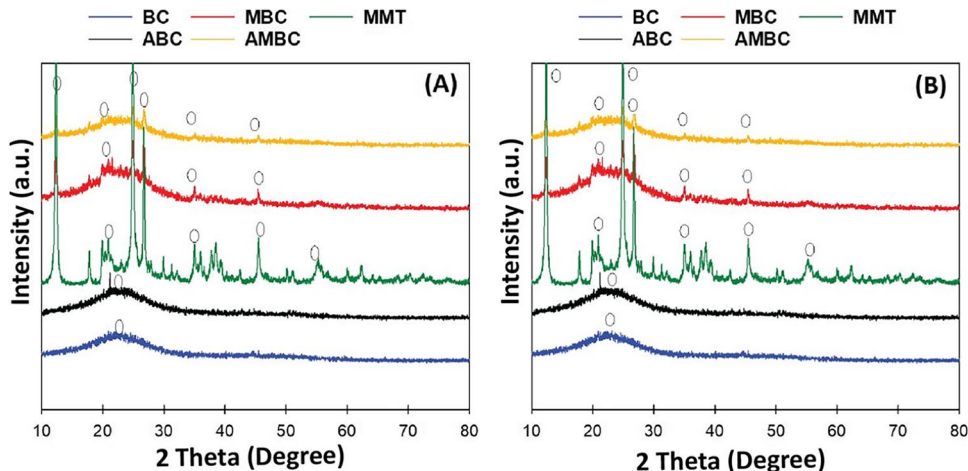
The existence of SiO_2 was shown by the presence of a broad hump at an angle of 2θ within the range of 22° in pristine and CO_2 activated BC, suggesting an amorphous carbon structure (Shi et al. 2019).

The Fourier transform infrared spectroscopy (FTIR) analysis (Fig. 4) revealed the presence of different functional groups that can be observed on the surface of as-synthesized materials. The peaks at wave numbers 466–470 cm^{-1}, 537 cm^{-1}, and 796–804 cm^{-1} were associated with Si–O-Si, Si–O-Al, and Si–O, respectively (Ramola et al. 2020). The development of conspicuous peaks between 1384 cm^{-1} and 1402 cm^{-1} might be the result of C-O stretching (Cao et al. 2019). Between 1597 cm^{-1} and 1636 cm^{-1}, the bands were ascribed to C=C/C=O, but with different intensities before and after the adsorption of AZT (Arif et al. 2022; Chen et al. 2017; Hou et al. 2021). The existence of –CH$_2$ groups is shown by the presence of peaks at 2923 cm^{-1} (Kim et al. 2012). All adsorbent materials exhibited peaks from 3405 cm^{-1} to 3439 cm^{-1}, indicating the existence of the O–H group. Peaks detected at 3621 to 3697 in the MBC and AMBC were slightly shifted to 3619–3696 cm^{-1} after AZT adsorption.

The X-Ray Photoemission Spectroscopy (XPS) analysis was utilized to determine the surface chemical characteristics of the as-synthesized materials. The XPS peak spectra revealed the presence of C1s, N1s, O1s, Al2p, and Si2p at

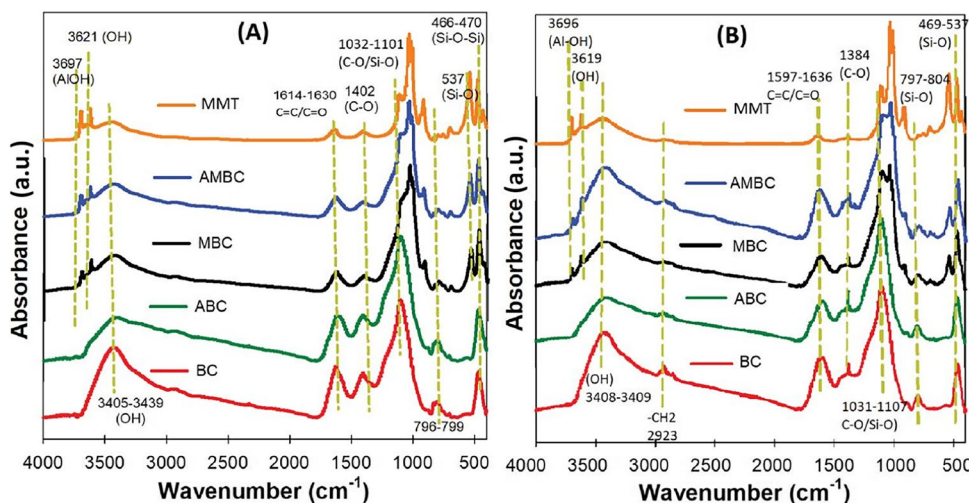**Fig. 4** FTIR analysis of different adsorbents before (**A**) and after (**B**) adsorption of AZT

Table 2 XPS analyses showing BE and atomic and peak area percentages (%) of various adsorbents

	Functional Groups	B.E. (eV)	BC	ABC	MBC	AMBC
C atomic %			71.1	70.3	56.1	60.7
Deconvoluted Peak area %	C-C/ C=C	284.7	47.0	50.0	49.0	49.0
	C-O/ C-N	285.7	19.0	17.0	19.0	20.0
	C=O	287.0	18.0	18.0	19.0	23.0
	COOH	289.3	16.0	15.0	13.0	11.0
O atomic %			20.8	21.7	26.5	29.3
Deconvoluted Peak area %	Al-O	531.2	2.0	4.0	7.0	6.0
	Si-O	532.3	16.0	13.0	42.0	34.0
	C-O	533.4	50.0	54.0	40.0	47.0
	COOH	534.5	32.0	29.0	12.0	13.0
N atomic %			1.1	0.6	0.6	0.9
Deconvoluted Peak area %	Pyridinic N	398.4	16.0	11.0	19.0	10.0
	Pyrrolic N	399.8	38.0	28.0	19.0	25.0
	Graphitic N	401.0	26.0	30.0	25.0	26.0
	Oxidized N	402.5	19.0	31.0	37.0	38.0
Si atomic %			7.0	7.1	8.9	8.9
	Si-O	103.7	6.0	39.0	86.0	78.0
	Si-OH	104.4	94.0	61.0	14.0	22.0
Al atomic %		75.1	---	---	5.2	4.0

284.8, 399–400, 532–534, 75.0, and 103–104 eV, respectively. The atomic and area percentages (%) of C1s, N1s, O1s, Al2p, and Si2p peaks for various materials are presented in Table 2. The atomic percentages of C, N, O, and Si were 71.05, 1.11, 20.85, and 6.99%, respectively, for BC. The main peak in the C1s region was deconvoluted into four peaks at 284.7, 285.7, 287, and 289.3 ascribed to C–C /C-Si/C=C, C-N/C-O, C=O, and COOH, accounting for 47, 19, 18, and 16% of the peak area, respectively (Lee et al. 2019). The changes in surface functional group contents after MMT treatment and activation with CO_2 indicated that some C=C bonding was shifted to an oxidized form that might be responsible for the removal of AZT.

Full-scan XPS spectra of all the prepared adsorbents before AZT adsorption were obtained (Fig. S1). The O1s peaks at 531.2 eV, 532.3 eV, 533.4 eV, and 534.5 eV were assigned to Al-O, Si-O, C-O, and COOH, having 2%, 16%, 50%, and 32% area, respectively (Mian et al. 2019). There were four peaks at 398.4 eV, 399.8 eV, 401.0 eV, and 402.5 eV. These peaks were for pyridinic, pyrrolic, graphitic, and oxidized N that had 16%, 38%, 26%, and 19% area, respectively, in the N1s peak (Mujtaba Munir et al. 2020). The oxidized N was increased in AMBC, which might be responsible for the degradation of AZT. The Si2p XPS spectrum indicated two peaks at 103.74 eV, and 104.45 eV, which can be assigned to Si-O and Si-OH (Arif et al. 2022). After modification with MMT, the atomic and area percentages of Al2p, Si2p, and O1s increased, showing that MMT was deposited onto the BC samples. Although the pure BC has less Al and Si, the composite contains a greater

concentration of these elements as a result of MMT. BC activation with CO_2 had little effect on the concentrations of any elements but did raise the total concentration of O, showing that CO_2 contributed to the augmentation of oxygen.

Effect of solution pH

Figure 5A presents the effect of solution pH on AZT removal and the adsorption behavior of this antibiotic on adsorbents including BC-500 and AMBC-500. The highest AZT adsorption by composite material was exhibited at pH 7, showing the strong electrostatic bond between AZT and the composite material. Whereas the adsorption capacity was slightly reduced at pH values greater or lower than 7, that might be due to surface charge repulsion. The pKa of AZT is 8.60 to 8.74, which is close to pH 7 and indicates that a large amount of AZT is dissociated into ions, which would favor the adsorption process. Moreover, if pH is greater than pKa (8.74), the dominant AZT species is negatively charged which involves repulsive electrostatic forces. When the pH is lower than the pKa value, AZT is in cationic form and is electrostatically attracted to the negatively charged BC surface (Tasić et al. 2018). At neutral pH, AZT mainly exists as a cation and its adsorption might be associated with cation exchange capacity (Hanamoto and Ogawa 2019). Adsorption of AZT increased significantly over the pH range of 3 to 7 and more than 80% of AZT from the solution was removed at this wide range of pH. However, the pH of equilibrium was 7, and maximum adsorption was observed at this pH. The tertiary amino group ($-NH(CH_3)_2$)

Fig. 5 Effect of solution pH (**A**), adsorbent dose (**B**), solution temperature (**C**), and contact time (**D**) on adsorption capacity of different adsorbents for removal of AZT
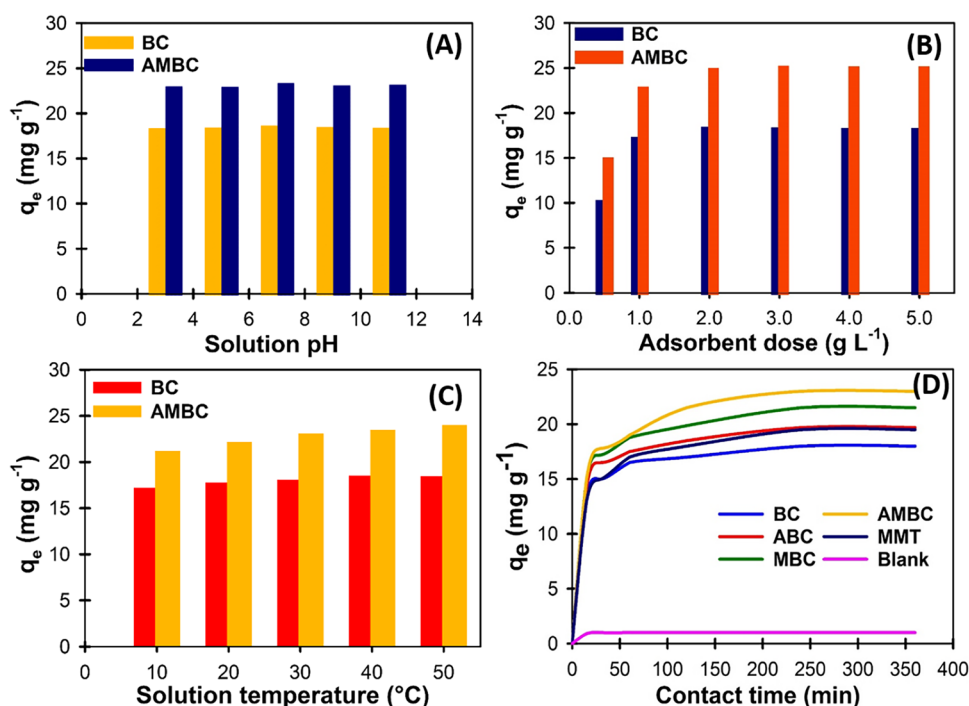
is a protonated form of AZT that is predominantly available at this pH (Vajdle et al. 2016). As a result of the electrostatic interaction and H-bonding mechanisms, it is thought that AZT and ≡S–O⁻ groups on the surface of the BC composite are attracted to each other. As the AZT molecule is very large and surface silanol groups (≡Si-OH) are supposed to be involved in the adsorption process (Sousa et al. 2018). The silanol groups are primarily negatively charged, they can interact with cationic compounds through additional ion-exchange processes.

Effect of adsorbent dose

The effectiveness of an adsorbent in the treatment of polluted water is mostly determined by the number of active adsorption sites accessible on the adsorbent surface (Hu et al. 2019; Oguntimein 2015). The impact of the adsorbent applied in the adsorption process is a significant factor indicating the adsorption capacity of the adsorbent for a defined contaminant concentration. It is also useful in dictating the sorbent–sorbate ratio in the removal process, as well as in cost forecasting for the removal process (Cheruiyot et al. 2019). The removal of AZT from contaminated water was affected by changing the adsorbent doses while keeping the other parameters constant as shown in Fig. 5B. The findings demonstrated that, to a certain degree, the removal of AZT rose as the adsorbent dosage increased. The removal of AZT was increased due to an increase in total surface area and accessibility of more active adsorption sites, thereby enhancing the adsorption of AZT. The AZT removal efficiency increased with increasing adsorbent dosage from 1 to 5 g L⁻¹, while the adsorption capacity was reduced owing to the increasing availability of unsaturated adsorption sites during the adsorption processes (Barquilha and Braga 2021).

Effect of temperature on AZT adsorption

During the adsorption process, the temperature is critical because it influences both the mobility and solubility of contaminant molecules in solution, as well as the surface characteristics of the adsorbent (Cheruiyot et al. 2019). Furthermore, increasing temperature causes an increase in the rate of diffusion of the adsorbate molecules across the external boundary layer of the adsorbent particles and inside their internal pores, which is followed by a reduced solution viscosity (Bouaziz et al. 2017). In industries and water purification plants, the optimum temperature at which the adsorption is most likely to be spontaneous is very important (Elwakeel et al. 2016). For these reasons, the effect of temperature on AZT removal by BC and AMBC was studied as shown in Fig. 5C.

The influence of temperature was investigated on the adsorption process in the range of 10–50 °C. As indicated, increasing the temperature increased AZT removal, with the maximum removal occurring at 50 °C. Generally, the adsorptive removal of contaminates rises as the solution temperature increases. This indicates that the adsorption process has an endothermic nature. The results obtained from this study were consistent with those of our previous study, which showed that the connection between antibiotics and active sites may be strengthened by increasing the temperature and may enhance adsorption (Arif et al. 2022). In contrast, the removal efficiency of AZT by organo-clays was found to decrease with an increase in solution temperature in a study conducted previously (Imanipoor et al. 2021).

Adsorption kinetics

The AZT removal rate is described by the kinetic studies in relation to variations in the AZT contact time on the adsorbent. Adequate kinetic models may be used to describe how several mechanisms, including surface adsorption, external diffusion, and/or pore diffusion, influence the transfer of AZT from the solution to the adsorbents at the same time. As shown in Fig. 6C and 6D, the effect of equilibrium time on the adsorption of AZT was investigated using BC and AMBC. The equilibrium time for AZT adsorption by all adsorbents may be described as having two phases, including primary fast adsorption followed by a second slower stage, with equilibrium occurring approximately after 6 h (Fig. 5D). The rapid adsorption process at the initial stage was perhaps due to larger number of adsorption sites, and ultimately the adsorption started to slow before reaching equilibrium (Guo et al. 2013). The data from the adsorption experiments were analyzed using PFO, PSO, and Elovich kinetic models to evaluate the kinetics of the process, as shown in Fig. 6C and D. The kinetic parameters defined by non-linear analysis are described in the supplementary material (Table S2). The values of R^2 acquired by the PSO model are 0.99 and 0.97 for BC and AMBC, respectively. Similarly, R^2 values of the Elovich model are 0.98 and 0.99 for BC and AMBC, respectively.

According to the PSO kinetic model, chemical adsorption involving valence forces via electron sharing or exchange between the AZT and adsorbents might be the rate-limiting phase (Chen et al. 2016). This occurs due to the presence of oxygenated functional groups that play a significant role in the adsorption of AZT. A chemical link formed between the AZT molecule and each of the multiple functional groups present on each of the active sites of AMBC during the adsorption process, and there was a direct relationship between adsorption capacity and the number of active sites present on the adsorbents. The studied adsorbents showed an Elovich fit, indicating the establishment of chemical interactions with the functional groups present on the AZT. Thus, the adsorption of AZT onto the as-synthesized adsorbents

Fig. 6 Non-linear adsorption isotherms for BC (**A**) and AMBC (**B**) and kinetics models for BC (**C**) and AMBC (**D**) synthesized at pyrolysis temperature of 500 °C
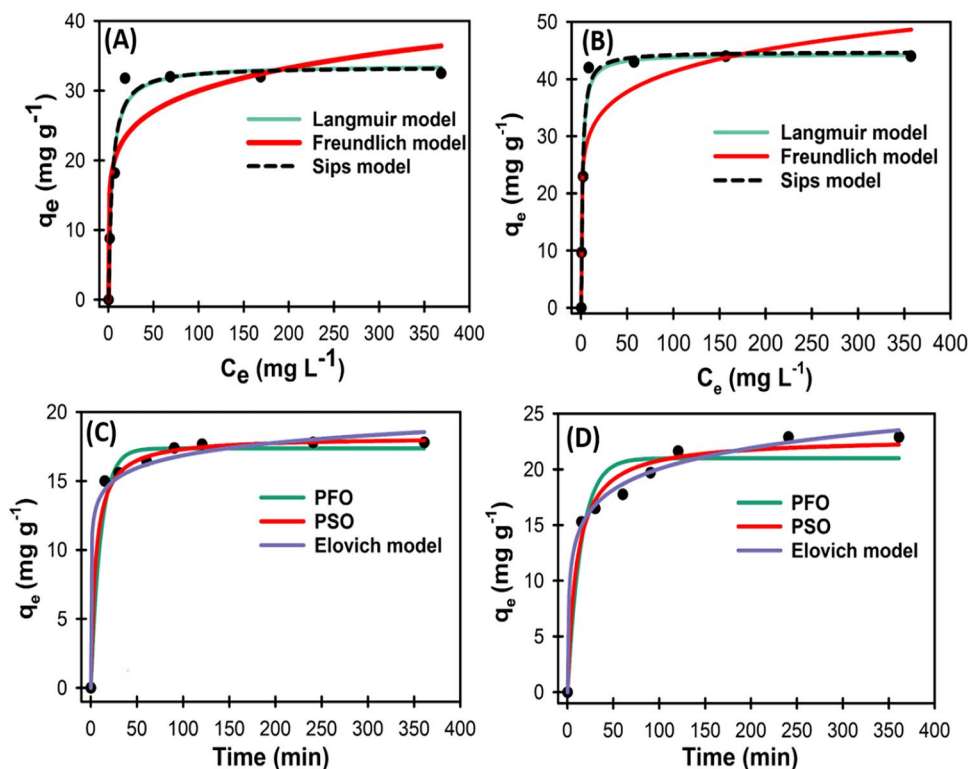
obeyed the PSO and Elovich kinetic models. It can be said that the AZT adsorption process on these adsorbents is a chemical one. Hydrogen bonds may be formed between the amine group of the AZT antibiotic and the oxygen present in the functional groups of the as-synthesized adsorbents, which may improve the removal efficiency (Imanipoor et al. 2021). The Elovich model is often used to explain chemical adsorption in which the rate decreases with time as the surface area of the substance increases. The Elovich model was the best match to represent the kinetic behavior of adsorbents in the AZT adsorption process in aqueous environment.

Adsorption isotherms

Adsorption isotherms represent the equilibrium relationship between the quantity of adsorbed material and its concentration in the bulk fluid phase at constant temperature (Sousa et al. 2018). The experimental data were fitted to Langmuir, Freundlich, and Sips isotherms and ismotherm parameters were derived using non-linear fitting of equation. The adsorption ability of BC and AMBC prepared at a pyrolysis temperature of 500 °C was investigated. It was observed that when the initial concentration of AZT was increased, an increasing amount of affinity for the adsorbent material was developed, which indicated that the binding sites were easily freely available to adsorbate. These results demonstrated that from 25 to 100 mg L^{-1}, the adsorption capacity rose significantly and then equilibrium was reached

due to saturation of binding sites. Adsorption equilibrium isotherms obtained from non-linear models are displayed in Fig. 6A and B for BC and AMBC, respectively.

The non-linear Langmuir and Sips models fit the experimental data better than the Freundlich models as their higher R^2 values (0.97). The Sips model combines the Langmuir and Freundlich expressions (Foo and Hameed 2010), therefore, the obtained results demonstrate that the AZT adsorption onto studied adsorbents is a complex process that cannot be described by basic isotherm models. In addition, the maximum adsorption capacities observed through these isotherms were quite close to the experimental values for BC and AMBC that were 32 and 44 mg g^{-1}, respectively. For AMBC and BC, the highest adsorption capacity determined using the Sips model was 44.73 and 33.4 mg g^{-1}, respectively (Table S1). The adsorbent surface was homogeneous, AZT molecules were adsorbed on the monolayer surface, and all active sites were energetically equal. The Langmuir model considers the adsorption of AZT as a chemisorption process through the sharing of electrons between the adsorbate and adsorbents (Sobhan Ardakani et al. 2020). The results obtained from adsorption models were consistent with the previous studies (Atugoda et al. 2021; Nassar et al. 2019). Adsorption on MMT happens primarily via three pathways: at the surface, on the edges of the plates, and in the interlayer gaps between two successive layers (Chen et al. 2016). Adsorption was boosted by electrostatic interactions between the functional groups of MMT and BC

molecules, which competed with the functional groups of AZT molecules during the whole adsorption process. The clay mineral has a lot of cationic groups that contribute to the coulombic interactions with the amide groups in AZT. The AZT was shown to be eliminated by AMBC via several interactions, including electrostatic interactions, ion exchange, hydrophobic interactions, and H-bonding, according to the findings of this study.

Electron Paramagnetic Resonance (EPR) analysis

The BC-based adsorbents exhibit catalytic activity due to the formation of free radicals. The EPR method, in combination with DMPO as a spin-tapping agent, was used to analyze the free radicals using various pH conditions and contact times. Time-dependent peaks of DMPO·OH are presented in Fig. 7A. It can be seen that there is not too much difference in peaks although the signals become weak over time, indicating that·OH produced in the system might be reduced over time, probably because of the deactivation of the corresponding active sites (Mian and Liu 2020). It also shows that catalytic activity is strongly dependent on the availability of catalytic active sites that are scattered across the interior pores (Lee et al. 2017). The peaks of·OH at various pH values can be seen in Fig. 7B. The presence of DMPO-·OH peaks at pH 11 was found to be significantly higher than those identified at pH 3, 5, 7, and 9. These findings revealed that AZT degradation was more severe under extremely basic conditions. Although pH affects the production of·OH, the change in pH did not influence the total removal of AZT. The degradation of AZT was examined using a scavenger test. The TBA was introduced as a scavenger to identify·OH and evaluate its function in the degradation of AZT. The results indicated that removal efficiency was decreased by 4.3% when compared to the control test, which did not include the use of any TBA. Following the results of the scavenging test, it was determined that the·OH was mainly involved in the AZT degradation. The results of the EPR analysis are consistent with the results of prior research in

which·OH was the primary contributor to the degradation of organic pollutants (Fu et al. 2015).

Compared to various research studies reported in the the previous literature, the adsorbent used in the current study has excellent adsorption capacity. For instance: zeolites used in a previous study adsorbed 7.56 mg g^{-1} AZT (Sousa et al. 2018). Similarly, PAC/Fe/Ag/Zn nanocomposite adsorption capacity for AZT was 14.18 mg g^{-1} reported in a previous study (Mehrdoost et al. 2022). The maximum adsorption capacity of clinoptilolite for AZT was 28.01 mg g^{-1} observed in a study (Saadi et al. 2021).

Conclusions

The removal of AZT from water using an inexpensive and environmentally friendly biochar impregnated with MMT and activated by CO_2 gas was investigated in this study. The characterization of the as-synthesized adsorbents was done using SEM, EDS, FTIR, Raman, EPR, XRD, BET, and TGA. The sorption process was primarily regulated by the solution pH, AZT concentration, contact duration, adsorbent dose, and solution temperature, as shown by the experimental findings. The equilibrium data were analyzed using the nonlinear Langmuir, Freundlich, and Sips isotherm models, which revealed that adsorption occurs in a homogenous manner. The monolayer adsorption capacity of BC and AMBC was found to be 33.4 mg g^{-1} and 44.73 mg g^{-1}, respectively. Kinetic studies identified that the experimental data obeyed the PSO and Elovich models, indicating the chemisorption nature of adsorbents. The thermodynamic parameters determine the endothermic and spontaneous nature of the reaction. The novel adsorbent, AMBC, exhibited excellent removal efficiency towards AZT. The ion exchange, π-π EDA interactions, H-bonding, and electrostatic interactions were the plausible mechanisms responsible for adsorption process. This study concluded that AMBC could be used as an effective, viable, and inexpensive adsorbent to remove AZT from contaminated water.

Fig. 7 EPR analysis of AMBC with (**A**) varying contact time and (**B**) pH
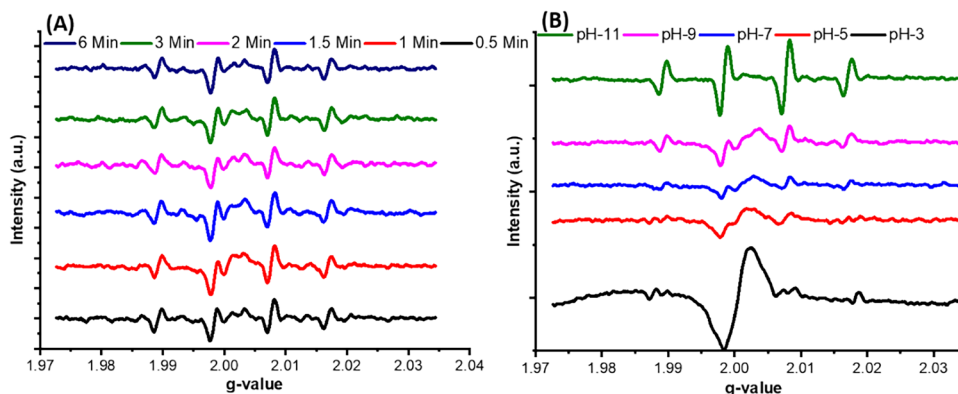
Further investigations are needed to assess the adsorption process using AMBC in a real-world situation. Future studies should address some issues, such as the cost–benefit analysis of AMBC applications, particularly in their regeneration techniques for adsorbent recycling; studies should be conducted at environmentally relevant concentrations and with more complex antibiotic mixtures.

Authors contributions Muhammad Arif: Writing original draft, Methodology, Formal analysis

Guijian Liu: Supervision, Funding acquisition
Muhammad Zia ur Rehman: Visualization, Editing
Md Manik Mian: Writing, Review and Editing
Aniqa Ashraf: Formal analysis, Validation
Balal Yousaf: Conceptualization
Muhammad Saqib Rashid: Experimental work, analysis
Rafay Ahmed: Software, Editing
Muhammad Imran: Writing, Review and Editing
Mehr Ahmed Mujtaba Munir: Software, Investigation

Data availability The data and materials were obtained from university of science and technology of China.

Declarations

Ethics approval All authors ensure that principles of ethical and professional conduct have been followed, information regarding sources of funding, potential conflicts of interest (financial or non-financial) are disclosed. No human or animal participation is involved in this work.

Consent to participate Not applicable.

Consent for publication Not applicable

Competing interest The authors declare no competing interests.

References

Alvarino T, Torregrosa N, Omil F, Lema JM, Suarez S (2017) Assessing the feasibility of two hybrid MBR systems using PAC for removing macro and micropollutants. J Environ Manage 203:831–837. https://doi.org/10.1016/j.jenvman.2016.03.023

Alves TC, Cabrera-Codony A, Barceló D, Rodriguez-Mozaz S, Pinheiro A, Gonzalez-Olmos R (2018) Influencing factors on the removal of pharmaceuticals from water with micro-grain activated carbon. Water Res 144:402–412. https://doi.org/10.1016/j.watres.2018.07.037

Amen R, Yaseen M, Mukhtar A, Klemeš JJ, Saqib S, Ullah S, Al-Sehemi AG, Rafiq S, Babar M, Fatt CL, Ibrahim M, Asif S, Qureshi KS, Akbar MM, Bokhari A (2020) Lead and cadmium removal from wastewater using eco-friendly biochar adsorbent derived from rice husk, wheat straw, and corncob. Clean Eng Technol 1:100006. https://doi.org/10.1016/j.clet.2020.100006

Andrade JR, Oliveira MF, da Silva MGC, Vieira MGA (2018) Adsorption of pharmaceuticals from water and wastewater using non-conventional low-cost materials: a review. Ind Eng Chem Res 57:3103–3127. https://doi.org/10.1021/acs.iecr.7b05137

Archer E, Petrie B, Kasprzyk-Hordern B, Wolfaardt GM (2017) The fate of pharmaceuticals and personal care products (PPCPs), endocrine disrupting contaminants (EDCs), metabolites and illicit drugs in a WWTW and environmental waters. Chemosphere 174:437–446. https://doi.org/10.1016/j.chemosphere.2017.01.101

Arif M, Liu G, Yousaf B, Ahmed R, Irshad S, Ashraf A, Zia-ur-Rehman M, Rashid MS (2021) Synthesis, characteristics and mechanistic insight into the clays and clay minerals-biochar surface interactions for contaminants removal-A review. J Clean Prod 310:127548. https://doi.org/10.1016/j.jclepro.2021.127548

Arif M, Liu G, Zia ur Rehman M, Yousaf B, Ahmed R, Mian MM, Ashraf A, Mujtaba Munir MA, Rashid MS, Naeem A (2022) Carbon dioxide activated biochar-clay mineral composite efficiently removes ciprofloxacin from contaminated water - Reveals an incubation study. J Clean Prod 332:130079. https://doi.org/10.1016/j.jclepro.2021.130079

Ashiq A, Adassooriya NM, Sarkar B, Rajapaksha AU, Ok YS, Vithanage M (2019a) Municipal solid waste biochar-bentonite composite for the removal of antibiotic ciprofloxacin from aqueous media. J Environ Manage 236:428–435. https://doi.org/10.1016/j.jenvman.2019.02.006

Ashiq A, Sarkar B, Adassooriya N, Walpita J, Rajapaksha AU, Ok YS, Vithanage M (2019b) Sorption process of municipal solid waste biochar-montmorillonite composite for ciprofloxacin removal in aqueous media. Chemosphere 236. https://doi.org/10.1016/j.chemosphere.2019.124384

Ashour S, Bayram R (2012) Novel spectrophotometric method for determination of some macrolide antibiotics in pharmaceutical formulations using 1,2-naphthoquinone-4-sulphonate. Spectrochim Acta Part A Mol Biomol Spectrosc 99:74–80. https://doi.org/10.1016/j.saa.2012.08.024

Ashraf A, Liu G, Yousaf B, Arif M, Ahmed R, Rashid A, Riaz L, Rashid MS (2022) Phyto-mediated photocatalysis: a critical review of in-depth base to reactive radical generation for erythromycin degradation. Environ Sci Pollut Res 29:32513–32544. https://doi.org/10.1007/s11356-022-19119-9

Ashraf A, Liu G, Yousaf B, Arif M, Ahmed R, Irshad S, Cheema AI, Rashid A, Gulzaman H (2021) Recent trends in advanced oxidation process-based degradation of erythromycin: pollution status, eco-toxicity and degradation mechanism in aquatic ecosystems. Sci Total Environ 145389. https://doi.org/10.1016/j.scitotenv.2021.145389

Atugoda T, Gunawardane C, Ahmad M, Vithanage M (2021) Mechanistic interaction of ciprofloxacin on zeolite modified seaweed (Sargassum crassifolium) derived biochar: kinetics, isotherm and thermodynamics. Chemosphere 281:130676. https://doi.org/10.1016/j.chemosphere.2021.130676

Avella AC, Delgado LF, Görner T, Albasi C, Galmiche M, de Donato P (2010) Effect of cytostatic drug presence on extracellular polymeric substances formation in municipal wastewater treated by membrane bioreactor. Bioresour Technol 101:518–526. https://doi.org/10.1016/j.biortech.2009.08.057

Barquilha CER, Braga MCB (2021) Adsorption of organic and inorganic pollutants onto biochars: challenges, operating conditions, and mechanisms. Bioresour Technol Rep 15:100728. https://doi.org/10.1016/j.biteb.2021.100728

Beltrame KK, Cazetta AL, de Souza PSC, Spessato L, Silva TL, Almeida VC (2018) Adsorption of caffeine on mesoporous activated carbon fibers prepared from pineapple plant leaves. Ecotoxicol Environ Saf 147:64–71. https://doi.org/10.1016/j.ecoenv.2017.08.034

Bouaziz F, Koubaa M, Kallel F, Ghorbel RE, Chaabouni SE (2017) Adsorptive removal of malachite green from aqueous solutions by almond gum: kinetic study and equilibrium isotherms. Int J Biol Macromol 105:56–65. https://doi.org/10.1016/j.ijbiomac.2017.06.106

Cano PA, Jaramillo-Baquero M, Zúñiga-Benítez H, Londoño YA, Peñuela GA (2020) Use of simulated sunlight radiation and hydrogen peroxide in azithromycin removal from aqueous solutions: optimization & mineralization analysis. Emerg Contam 6:53–61. https://doi.org/10.1016/j.emcon.2019.12.004

Cao Y, Shen G, Zhang Y, Gao C, Li Y, Zhang P, Xiao W, Han L (2019) Impacts of carbonization temperature on the Pb(II) adsorption by wheat straw-derived biochar and related mechanism. Sci Total Environ 692:479–489. https://doi.org/10.1016/j.scitotenv.2019.07.102

Carrasquillo AJ, Bruland GL, MacKay AA, Vasudevan D (2008) Sorption of ciprofloxacin and oxytetracycline zwitterions to soils and soil minerals: influence of compound structure. Environ Sci Technol 42:7634–7642. https://doi.org/10.1021/es801277y

Chang Y, Wang L-X, Li Y-P, Hu C-Q (2015) Factors influencing the HPLC determination for related substances of azithromycin. J Chromatogr Sci 54:bmv127. https://doi.org/10.1093/chromsci/bmv127

Chen L, Zhou CH, Fiore S, Tong DS, Zhang H, Li CS, Ji SF, Yu WH (2016) Functional magnetic nanoparticle/clay mineral nanocomposites: preparation, magnetism and versatile applications. Appl Clay Sci 127–128:143–163. https://doi.org/10.1016/j.clay.2016.04.009

Chen L, Long X, Hui C, Min H, Fu S (2017) Environmental-friendly montmorillonite-biochar composites: facile production and tunable adsorption-release of ammonium and phosphate. J Clean Prod 156:648–659. https://doi.org/10.1016/j.jclepro.2017.04.050

Cheruiyot GK, Wanyonyi WC, Kiplimo JJ, Maina EN (2019) Adsorption of toxic crystal violet dye using coffee husks: equilibrium, kinetics and thermodynamics study. Sci Afr 5:e00116. https://doi.org/10.1016/j.sciaf.2019.e00116

Davoodi S, Dahrazma B, Goudarzi N, Gorji HG (2019) Adsorptive removal of azithromycin from aqueous solutions using raw and saponin-modified nano diatomite. Water Sci Technol 80:939–949. https://doi.org/10.2166/wst.2019.337

Dehghan A, Mohammadi AA, Yousefi M, Najafpoor AA, Shams M, Rezania S (2019) Enhanced kinetic removal of ciprofloxacin onto metal-organic frameworks by sonication, process optimization and metal leaching study. Nanomater. (Basel, Switzerland) 9:1422. https://doi.org/10.3390/nano9101422

Elwakeel KZ, El-Kousy S, El-Shorbagy HG, El-Ghaffar MAA (2016) Comparison between the removal of Reactive Black 5 from aqueous solutions by 3-amino-1,2,4 triazole,5-thiol and melamine grafted chitosan prepared through four different routes. J Environ Chem Eng 4:733–745. https://doi.org/10.1016/j.jece.2015.12.015

Feng K, Xu Z, Gao B, Xu X, Zhao L, Qiu H, Cao X (2021) Mesoporous ball-milling iron-loaded biochar for enhanced sorption of reactive red: Performance and mechanisms. Environ Pollut 290:117992. https://doi.org/10.1016/j.envpol.2021.117992

Foo KY, Hameed BH (2010) Insights into the modeling of adsorption isotherm systems. Chem Eng J 156:2. https://doi.org/10.1016/j.cej.2009.09.013

Fu X, Gu X, Lu S, Miao Z, Xu M, Zhang X, Qiu Z, Sui Q (2015) Benzene depletion by Fe2+-catalyzed sodium percarbonate in aqueous solution. Chem Eng J 267:25–33. https://doi.org/10.1016/j.cej.2014.12.104

Guo X, Yang C, Dang Z, Zhang Q, Li Y, Meng Q (2013) Sorption thermodynamics and kinetics properties of tylosin and sulfamethazine on goethite. Chem Eng J 223:59–67. https://doi.org/10.1016/j.cej.2013.02.115

Gupta A, Garg A (2019) Adsorption and oxidation of ciprofloxacin in a fixed bed column using activated sludge derived activated carbon. J Environ Manage 250:109474. https://doi.org/10.1016/j.jenvman.2019.109474

Hanamoto S, Ogawa F (2019) Predicting the sorption of azithromycin and levofloxacin to sediments from mineral and organic components. Environ Pollut 255:113180. https://doi.org/10.1016/j.envpol.2019.113180

Hossain N, Nizamuddin S, Griffin G, Selvakannan P, Mubarak NM, Mahlia TMI (2020) Synthesis and characterization of rice husk biochar via hydrothermal carbonization for wastewater treatment and biofuel production. Sci Rep 10:18851. https://doi.org/10.1038/s41598-020-75936-3

Hou Y, Liang Y, Hu H, Tao Y, Zhou J, Cai J (2021) Facile preparation of multi-porous biochar from lotus biomass for methyl orange removal: Kinetics, isotherms, and regeneration studies. Bioresour Technol 329:124877. https://doi.org/10.1016/j.biortech.2021.124877

Hu Y, Zhu Y, Zhang Y, Lin T, Zeng G, Zhang S, Wang Y, He W, Zhang M, Long H (2019) An efficient adsorbent: simultaneous activated and magnetic ZnO doped biochar derived from camphor leaves for ciprofloxacin adsorption. Bioresour Technol 288:121511. https://doi.org/10.1016/j.biortech.2019.121511

Huang W, Chen J, Zhang J (2020) Removal of ciprofloxacin from aqueous solution by rabbit manure biochar. Environ Technol 41:1380–1390. https://doi.org/10.1080/09593330.2018.1535628

Imanipoor J, Mohammadi M, Dinari M (2021) Evaluating the performance of L-methionine modified montmorillonite K10 and 3-aminopropyltriethoxysilane functionalized magnesium phyllosilicate organoclays for adsorptive removal of azithromycin from water. Sep Purif Technol 275. https://doi.org/10.1016/j.seppur.2021.119256

Kim KH, Kim J-Y, Cho T-S, Choi JW (2012) Influence of pyrolysis temperature on physicochemical properties of biochar obtained from the fast pyrolysis of pitch pine (Pinus rigida). Bioresour Technol 118:158–162. https://doi.org/10.1016/j.biortech.2012.04.094

Kołtowski M, Hilber I, Bucheli TD, Charmas B, Skubiszewska-Zięba J, Oleszczuk P (2017) Activated biochars reduce the exposure of polycyclic aromatic hydrocarbons in industrially contaminated soils. Chem Eng J 310:33–40. https://doi.org/10.1016/j.cej.2016.10.065

Langmuir I (1916) The constitution and fundamental properties of solids and liquids. Part I. Solids J Am Chem Soc 38:2221–2295. https://doi.org/10.1021/ja02268a002

Lee J, Kim K-H, Kwon EE (2017) Biochar as a catalyst. Renew Sustain Energy Rev 77:70–79. https://doi.org/10.1016/j.rser.2017.04.002

Lee SY, Choi J-W, Song KG, Choi K, Lee YJ, Jung K-W (2019) Adsorption and mechanistic study for phosphate removal by rice husk-derived biochar functionalized with Mg/Al-calcined layered double hydroxides via co-pyrolysis. Compos Part B Eng. 176:107209. https://doi.org/10.1016/j.compositesb.2019.107209

Li J, Pan L, Yu G, Xie S, Li C, Lai D, Li Z, You F, Wang Y (2019) The synthesis of heterogeneous Fenton-like catalyst using sewage sludge biochar and its application for ciprofloxacin degradation. Sci Total Environ 654:1284–1292. https://doi.org/10.1016/j.scitotenv.2018.11.013

Li D, Zhou H, Huang L, Zhang J, Cui J, Li X (2021) Role of adsorption during nanofiltration of sulfamethoxazole and azithromycin solution. Sep Sci Technol 56:1996–2010. https://doi.org/10.1080/01496395.2020.1806326

Ma Y, Li M, Li P, Yang L, Wu L, Gao F, Qi X, Zhang Z (2021) Hydrothermal synthesis of magnetic sludge biochar for tetracycline and ciprofloxacin adsorptive removal. Bioresour Technol 319:124199. https://doi.org/10.1016/j.biortech.2020.124199

Mehrdoost A, Yengejeh RJ, Mohammadi MK et al (2022) Adsorption removal and photocatalytic degradation of azithromycin from aqueous solution using PAC/Fe/Ag/Zn nanocomposite. Environ Sci Pollut Res 29:33514–33527. https://doi.org/10.1007/s11356-021-18158-y

Mian MM, Liu G (2020) Activation of peroxymonosulfate by chemically modified sludge biochar for the removal of organic pollutants: understanding the role of active sites and mechanism. Chem Eng J 392:123681. https://doi.org/10.1016/j.cej.2019.123681

Mian MM, Liu G, Fu B, Song Y (2019) Facile synthesis of sludge-derived MnOx-N-biochar as an efficient catalyst for peroxymonosulfate activation. Appl Catal B Environ 255:117765. https://doi.org/10.1016/j.apcatb.2019.117765

Mujtaba Munir MA, Liu G, Yousaf B, Ali MU, Abbas Q, Ullah H (2020) Synergistic effects of biochar and processed fly ash on bioavailability, transformation and accumulation of heavy metals by maize (Zea mays L.) in coal-mining contaminated soil. Chemosphere 240. https://doi.org/10.1016/j.chemosphere.2019.124845

Nassar MY, Ahmed IS, Raya MA (2019) A facile and tunable approach for synthesis of pure silica nanostructures from rice husk for the removal of ciprofloxacin drug from polluted aqueous solutions. J Mol Liq 282:251–263. https://doi.org/10.1016/j.molliq.2019.03.017

Oguntimein GB (2015) Biosorption of dye from textile wastewater effluent onto alkali treated dried sunflower seed hull and design of a batch adsorber. J Environ Chem Eng 3:2647–2661. https://doi.org/10.1016/j.jece.2015.09.028

Ouasfi N, Zbair M, Bouzikri S, Anfar Z, Bensitel M, Ait Ahsaine H, Sabbar E, Khamliche L (2019) Selected pharmaceuticals removal using algae derived porous carbon: experimental, modeling and DFT theoretical insights. RSC Adv 9:9792–9808. https://doi.org/10.1039/C9RA01086F

Peng B, Chen L, Que C, Yang K, Deng F, Deng X, Shi G, Xu G, Wu M (2016) Adsorption of antibiotics on graphene and biochar in aqueous solutions induced by π-π interactions. Sci Rep 6:31920. https://doi.org/10.1038/srep31920

Ramola S, Belwal T, Jun C, Ying Y, Hao H, Mao S, Hui C (2020) Improved lead removal from aqueous solution using novel porous bentonite - and calcite-biochar composite. Sci Total Environ 709. https://doi.org/10.1016/j.scitotenv.2019.136171

Rawal A, Joseph SD, Hook JM, Chia CH, Munroe PR, Donne S, Lin Y, Phelan D, Mitchell DRG, Pace B, Horvat J, Webber JBW (2016) Mineral-biochar composites: molecular structure and porosity. Environ Sci Technol 50:7706–7714. https://doi.org/10.1021/acs.est.6b00685

Saadi Z, Fazaeli R, Vafajoo L, Naser I, Mohammadi G (2020) Promotion of clinoptilolite adsorption for azithromycin antibiotic by Tween 80 and Triton X-100 surface modifiers under batch and fixed-bed processes. Chem Eng Commun 6445:1–21. https://doi.org/10.1080/00986445.2020.1715955

Saadi Z, Fazaeli R, Vafajoo L, Naser I, Mohammadi G (2021) Promotion of clinoptilolite adsorption for azithromycin antibiotic by Tween 80 and Triton X-100 surface modifiers under batch and fixed-bed processes. Chem Eng Commun 208:328–348. https://doi.org/10.1080/00986445.2020.1715955

Senta I, Kostanjevecki P, Krizman-Matasic I, Terzic S, Ahel M (2019) Occurrence and behavior of macrolide antibiotics in municipal wastewater treatment: possible importance of metabolites, synthesis byproducts, and transformation products. Environ Sci Technol 53:7463–7472. https://doi.org/10.1021/acs.est.9b01420

Shi J, Fan X, Tsang DCW, Wang F, Shen Z, Hou D, Alessi DS (2019) Removal of lead by rice husk biochars produced at different temperatures and implications for their environmental utilizations. Chemosphere 235:825–831. https://doi.org/10.1016/j.chemosphere.2019.06.237

Silva CF, Deutschendorf C, Nagel FM, Dalmora CH, dos Santos RP, Lisboa TC (2021) Impact of the pandemic on antimicrobial consumption patterns. Infect Control Hosp Epidemiol 42:1170–1172. https://doi.org/10.1017/ice.2020.1227

Sobhan Ardakani S, Cheraghi M, Jafari A, Zandipak R (2020) PECVD synthesis of ZnO/Si thin film as a novel adsorbent for removal of azithromycin from water samples. Int J Environ Anal Chem:1–18. https://doi.org/10.1080/03067319.2020.1793973

Song J, Zhang S, Li G, Du Q, Yang F (2020) Preparation of montmorillonite modified biochar with various temperatures and their mechanism for Zn ion removal. J Hazard Mater 391:121692. https://doi.org/10.1016/j.jhazmat.2019.121692

Sophia AC, Lima EC (2018) Removal of emerging contaminants from the environment by adsorption. Ecotoxicol Environ Saf 150(1):17. https://doi.org/10.1016/j.ecoenv.2017.12.026

Sousa DNR, Insa S, Mozeto AA, Petrovic M, Chaves TF, Fadini PS (2018) Equilibrium and kinetic studies of the adsorption of antibiotics from aqueous solutions onto powdered zeolites. Chemosphere 205:137–146. https://doi.org/10.1016/j.chemosphere.2018.04.085

Sun C, Chen T, Huang Q, Zhan M, Li X, Yan J (2020) Activation of persulfate by CO2-activated biochar for improved phenolic pollutant degradation: performance and mechanism. Chem Eng J 380:122519. https://doi.org/10.1016/j.cej.2019.122519

Talaiekhozani A, Joudaki S, Banisharif F, Eskandari Z, Cho J, Moghadam G, Rezania S (2020) Comparison of azithromycin removal from water using UV radiation, Fe (VI) oxidation process and ZnO nanoparticles. Int J Environ Res Public Health 17. https://doi.org/10.3390/ijerph17051758

Tasić ŽZ, Petrović Mihajlović MB, Radovanović MB, Antonijević MM (2018) Electrochemical investigations of copper corrosion inhibition by azithromycin in 0.9% NaCl. J Mol Liq 265:687–692. https://doi.org/10.1016/j.molliq.2018.03.116

Vajdle O, Guzsvány V, Škorić D, Anojčić J, Jovanov P, Avramov-Ivić M, Csanádi J, Kónya Z, Petrović S, Bobrowski A (2016) Voltammetric behavior of erythromycin ethylsuccinate at a renewable silver-amalgam film electrode and its determination in urine and in a pharmaceutical preparation. Electrochim Acta 191:44–54. https://doi.org/10.1016/j.electacta.2015.12.207

Vermillion Maier ML, Tjeerdema RS (2018) Azithromycin sorption and biodegradation in a simulated California river system. Chemosphere 190:471–480. https://doi.org/10.1016/j.chemosphere.2017.10.008

Viglašová E, Galamboš M, Danková Z, Krivosudský L, Lengauer CL, Hood-Nowotny R, Soja G, Rompel A, Matík M, Briančin J (2018) Production, characterization and adsorption studies of bamboo-based biochar/montmorillonite composite for nitrate removal. Waste Manag 79:385–394. https://doi.org/10.1016/j.wasman.2018.08.005

Vikrant K, Kim K-H, Kwon EE, Boukhvalov DW (2022) Reactive adsorption and catalytic oxidation of gaseous formaldehyde at room temperature by a synergistic copper-magnesium bimetal oxide biochar composite. Chem Eng J 433:133497. https://doi.org/10.1016/j.cej.2021.133497

Wu F-C, Tseng R-L, Juang R-S (2009) Characteristics of Elovich equation used for the analysis of adsorption kinetics in dye-chitosan systems. Chem Eng J 150:366–373. https://doi.org/10.1016/j.cej.2009.01.014

Wu FC, Wu PH, Tseng RL, Juang RS (2014) Use of refuse-derived fuel waste for the adsorption of 4-chlorophenol and dyes from aqueous solution: equilibrium and kinetics. J Taiwan Inst Chem Eng 45:2628–2639. https://doi.org/10.1016/j.jtice.2014.07.007

Xiang JJ, Zha Xi CD, Liao QG, Yuan LJ, Zhang DW (2020) Detection of azithromycin residue in broiler feathers by liquid chromatography-tandem mass spectrometry. J Chromatogr B 1152:122225. https://doi.org/10.1016/j.jchromb.2020.122225

Yang Z, Xu X, Dai M, Wang L, Shi X, Guo R (2017) Accelerated ciprofloxacin biodegradation in the presence of magnetite nanoparticles. Chemosphere 188:168–173. https://doi.org/10.1016/j.chemosphere.2017.08.159

Yang X, Liu Z, Jiang Y, Li F, Xue B, Dong Z, Ding M, Chen R, Yang Q, An T, Shao X, Wang L (2020) Micro-structure, surface properties and adsorption capacity of ball-milled cellulosic biomass derived biochar based mineral composites synthesized via carbon-bed pyrolysis. Appl Clay Sci 199:105877. https://doi.org/10.1016/j.clay.2020.105877

Yao Y, Gao B, Fang J, Zhang M, Chen H, Zhou Y, Creamer AE, Sun Y, Yang L (2014) Characterization and environmental applications of clay–biochar composites. Chem Eng J 242:136–143. https://doi.org/10.1016/j.cej.2013.12.062

Yi S, Gao B, Sun Y, Wu J, Shi X, Wu B, Hu X (2016) Removal of levofloxacin from aqueous solution using rice-husk and wood-chip biochars. Chemosphere 150:694–701. https://doi.org/10.1016/j.chemosphere.2015.12.112

Yin D, Xu Z, Shi J, Shen L, He Z (2018) Adsorption characteristics of ciprofloxacin on the schorl: kinetics, thermodynamics, effect of metal ion and mechanisms. J Water Reuse Desalin 8:350–359. https://doi.org/10.2166/wrd.2017.143

Zango ZU, Garba A, Garba ZN, Zango MU, Usman F, Lim J-W (2022) Montmorillonite for adsorption and catalytic elimination of pollutants from Wastewater: a State-of-the-Arts review. Sustain 14:16441. https://doi.org/10.3390/su142416441

Zhang C-L, Qiao G-L, Zhao F, Wang Y (2011) Thermodynamic and kinetic parameters of ciprofloxacin adsorption onto modified coal fly ash from aqueous solution. J Mol Liq 163:53–56. https://doi.org/10.1016/j.molliq.2011.07.005

Zhang Y, Cao B, Zhao L, Sun L, Gao Y, Li J, Yang F (2018) Biochar-supported reduced graphene oxide composite for adsorption and coadsorption of atrazine and lead ions. Appl Surf Sci 427:147–155. https://doi.org/10.1016/j.apsusc.2017.07.237

Zhang R, Zheng X, Chen B, Ma J, Niu X, Zhang D, Lin Z, Fu M, Zhou S (2020) Enhanced adsorption of sulfamethoxazole from aqueous solution by Fe-impregnated graphited biochar. J Clean Prod 256:120662. https://doi.org/10.1016/j.jclepro.2020.120662

Zhou C-H, Zhang D, Tong D-S, Wu L-M, Yu W-H, Ismadji S (2012) Paper-like composites of cellulose acetate–organo-montmorillonite for removal of hazardous anionic dye in water. Chem Eng J 209:223–234. https://doi.org/10.1016/j.cej.2012.07.107